HEFAT2014
10th International Conference on Heat Transfer, Fluid Mechanics and Thermodynamics
14 – 16 July 2014
Orlando, Florida

MULTIPHASE FLOW AND HEAT TRANSFER ON MICRO/NANOSTRUCTURED SURFACES

H.H. Qiu*
*Author for correspondence
Department of Mechanical and Aerospace Engineering,
The Hong Kong University of Science and Technology,
Clear Water Bay, Kowloon
Hong Kong SAR, China
E-mail: meqiu@ust.hk

ABSTRACT

Multiphase flow and heat transfer in mini/microspaces are of significant interest for thermal management applications, where the latent heat of phase change offers an efficient method to dissipate large heat fluxes in a compact device, such as a heat spreader or a heat pipe. However, a significant challenge for the implementation of microscale phase change heat spreader is associated with micro/nano flow instabilities due to insufficient micro/nano bubble removal, leading to local liquid dry-out which severely limits the heat removal efficiency. This work will conduct a review on the challenges and opportunities that surfaces with micro/nanostructure patterned wettabilities. Bubble dynamics, fluid flow and heat transfer caused by the micro/nanostructure patterned surfaces will be reported and discussed. The effects of micro/nanostructure patterned surfaces on flow generation under a vapor bubble in a microchannel under very low Reynolds number will be demonstrated. The effects of wettability patterned surfaces on nucleation pool boiling and flow boiling heat transfer processes will be described. Bubble formation, breakup and departure are visualized and measured. Wettability patterned micro/nanostructure surfaces are manufactured on glass wafers and copper surfaces, respectively. Different surface hexagonal pattern size will be used. Indium Tin Oxide (ITO), Fluoroalkylsilanes (FAS) and Copper Oxide (CuO) will be used for glass and copper surfaces, respectively. It is found that bubble dynamics and pool boiling performance are enhanced significantly on smooth and flat surfaces combining hydrophilic and hydrophobic patterns in comparison with a hydrophilic surface. A micro/nanostructured heat spreader with asymmetrical wettability patterns will be demonstrated.

INTRODUCTION

Pool Boiling and flow boiling are efficient techniques to remove large amounts of heat at a prescribed temperature because of the large latent heat of vaporization. A boiling heat transfer system is normally considered that of an intermediate fluid on a solid surface, where there are triple contact lines that are the inter-connected lines for all three phases; liquid, gas, and solid. The triple contact lines can be dynamically expanded, shrunken, and moved during the nucleation, bubble formation and break-up processes under pool boiling or flow boiling conditions. This dynamic motion of the triple contact lines should be balanced with a dynamic contact, which is governed by the wettability. Thus, the wettability has a potential of being effective parameter in the heat transfer, especially a multiphase heat transfer. Many heat transfer systems become smaller, governing forces change from a body force to a surface force. This means that an interfacial force is predominant. Thus, the wettability becomes also one of influential parameters in the heat transfer. Specifically, on a nano- and micro-metric scale, the relative importance of surface tension and viscous forces become predominant compared to inertia and buoyancy forces. Because the instability of micro/nanobubble formation and breakup is sensitive to the interfacial surface tension, and the temperature distribution, due to the wettability of the surface, the capillary forces are particularly sensitive to the geometry of the surface wettability patterns. In multiphase flow and heat transfer, vapor bubbles generated on the micro/nanostructure wettability patterned surfaces may create instability of bubble dynamics that may have the potential to enhance heat transfer and critical heat flux from the surfaces. To address this challenge, several techniques have been proposed to enhance two-phase flow and heat transfer in mini/microspaces. Boiling in microscale is very complex phenomena which involves onset of nucleation, bubble growth and departure of vapor bubbles and is much different in the case of macroscale [1]. Key three parameters used to evaluation of boiling heat transfer in microchannel typically include onset of nucleation (ONB), two-phase heat transfer coefficient (HTC) and critical heat flux CHF) [2, 3]. Kuo et al. used the structured reentrant cavities to

promote nucleation in microchannel and reduce the boiling inception [4], such kind of this generation artificial nucleation also includes micro pin fins [5, 6], and single artificial cavity [7]. Morshed and Li used different methods to fabricate the nanowire in microchannel to modify to character of microchannel, their results shown that nanowire can make a significant enhancement in heat transfer performance and suppress the pressure oscillation the microchannel [8, 9]. Liu et al stated that the surface wettability effect can be ignored in flow boiling in microchannel [10]. This may be due to the difficulty of fabrication and surface modification in microscale [11]. Various heat transfer applications related with these special surfaces are accelerated by new micro/nano structured surface fabrication techniques, because the surface wettability can be changed by only different material deposition [12]. Recently Betz [13] showed a promising result of pool boiling on a heterogeneous wettability surface and large enhancements of critical heat flux and heat transfer coefficient are typically found for hydrophilic networks featuring hydrophobic islands.

POOL BOILING ON MICROSTRUCTED SURFACES

Boiling is most often understood as a phase transition from a liquid state to a vapor state involving the appearance of vapor bubbles on a hot surface. In this respect, forced convection boiling (flow boiling) and pool boiling have much in common. However, forced convection imparts a number of specific features to the conditions of bubble production and breakaway into the bulk of the liquid. The structures of vapor-liquid mixtures resulting from boiling and mixing of liquid and vapor phases also differ appreciably from each other. Usually, flow boiling caused forced convection intensifies these processes compared to free motion accompanying pool boiling. Therefore, the term flow boiling describes the boiling of bulk liquids forced to move along hot surfaces, while in pool boiling, the liquid is stagnant [14] and in contact with a hot solid surface or a liquid whose flow results from natural convection. These definitions well describe the flow boiling and pooling at macroscale. This is because the common assumption in boiling studies is that the surface has a unique value of wettability. However, when a boiling process is taken place on a micro/ nanostructured surface, especially, on a micro/nanostructure patterned surface, the similarity between flow boiling and pool boiling becomes significant because the unbalanced capillary force will induce local flow near the nucleation sites which will significantly enhance heat transfer coefficient for pool boiling as well as flow boiling processes.

The performance of pool boiling is measured with two parameters, the heat transfer coefficient and the critical heat flux. The critical heat flux occurs due to the formation of a vapor film insulating the liquid from the heated surface, a phenomenon called dry out. Several characteristics determine the performance of a boiling surface. Nucleation sites in appropriate number and dimensions need to be provided such as cavities, rough areas, or hydrophobic islands [15]. Normally, using wicking structures can prevent dry out [16]. Other surface modifications are by increasing the surface area with fins or fluidized bed [16-19] and by enhancing the wettability of the surface [18-23]. The latter strategy is justified by experiments of Wang and Dhir [24], showing that the critical heat flux was increased by enhancing surface wettability. Significant heat transfer enhancement has also been obtained with surfaces coated with a micrometer thick carpet of nanometer diameter rods nanorods [18-20]. The critical heat flux enhancement was attributed to coupled effects such as the multiscale geometry [18, 20] and the superhydrophilicity of the nanowire arrays [19]. Although it was assumed that hydrophobic zones will promote nucleation, while the surface hydrophilicity enhance the critical heat flux, due to the complexity of the microscale effects, the influences of microstructured wettability on pool boiling were not well understood. Particularly, under a well-designed hydrophobic/hydrophilic micro-network, the mechanisms of heat transfer enhancement on pool boiling need to be further investigated.

Experimental Setup

To have a better understanding on the nucleation enhancement of wettability patterned surfaces [13], a transparent chamber was built to observe the bubble dynamics inside the mimic vapor chamber. Indium-tin-oxide (ITO) glass is used as the substrate because of its optical transparency and electrical conductivity. The ITO layer was etched leaving an area of $1mm^2$ to mimic the heater as mentioned above whose resistance is around 20Ω. There are three chambers with different surface wetting properties. The first one is the hydrophilic ITO surface, the second one is the hydrophobic surface coated with FAS and there're hydrophobic patterns on the hydrophilic surface for the third one as shown in Figure 1.

The FAS patterns are formed by 100μm×100μm hydrophobic array with a space of 200 μm. DI water is used as working fluid in the chamber and the input power density for the heater ranges from $30W/cm^2$ to $550W/cm^2$. The schematic of the experimental setup was show as Figure 1. High speed camera (MotionXtra HG-100K, Redlake Co.) was used to capture bubble behaviors such as bubble departure diameter, bubble departure period and active nucleation site density. Signal generator and an amplifier were used as power supply. Square wave with frequency of 1 kHz was used in the experiments. The heat flux was measured from voltage supply to the heater and the current. Voltages were recorded by Data Acquisition Switch Unit (Agilent 34970A). Degased DI water (boiled for more than 2 hours) with room temperature (25°C) was used as working fluid in the pool. A certain volume (1.5cm height) of water was used in each experiment for repeatability.

Number of nucleation sites

Pool boiling on a smooth ITO surface was investigated for comparison first. The heat flux supplied was $139W/cm^2$. As shown in Figure 3, bubble nucleation appeared as a single bubble growth against time and, eventually, the bubble size becomes comparable to the ITO heater surface area ($1mm^2$). In this case no other nucleation site was observed.

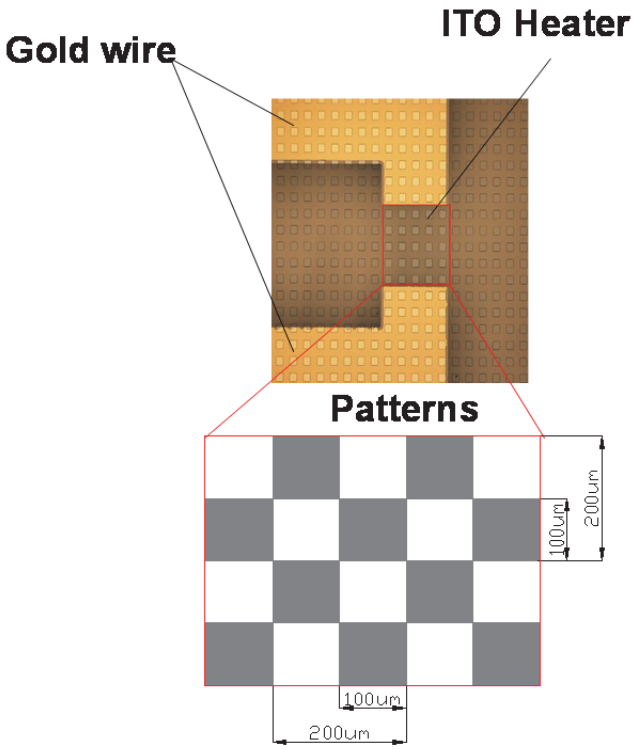

Figure 1 A wettability patterned ITO surface (Total area:1mm×1mm)

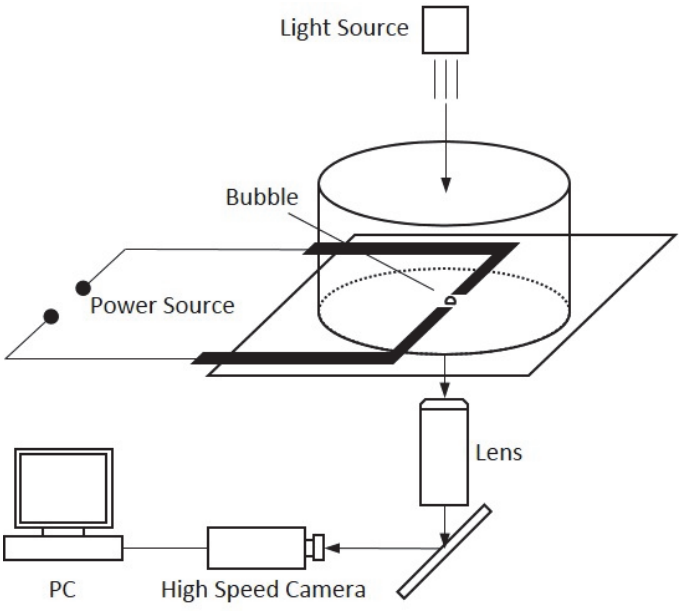

Figure 1 Schematic of the experimental setup

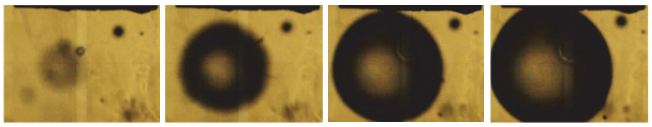

Figure 3 Bubble nucleation on a monophilic surface and its diameter increased against time; (a) ~ (d) heat flux: = 139W/cm^2

Dry-out was observed when the heat flux reached 293W/cm^2 as shown in Figure 4.

Figure 4 Dry-out on a hydrophilic surface

The microstructure patterned surface in Figure 1 was characterized in the pool boiling setup described in Figure 2, allowing for high speed visualization and measurements of heat flux vs. nucleation sites. In Fig. 5, a high speed camera is used to characterize the incipience of boiling, i.e., the density of active nucleation sites as a function of the surface heat flux. Because of confined shape and size of the hydrophobic islands fabricated on the substrate, nucleate sites of bubbles were precisely controlled on the islands during boiling (see Figure 5).

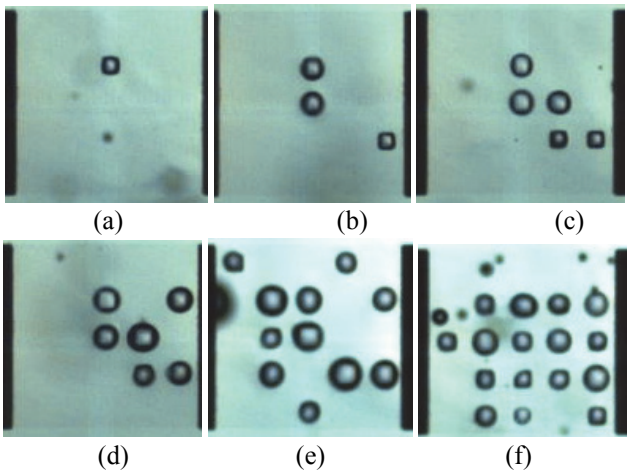

Figure 5 Number of nucleation sites increased with increasing of heat flux: (a) 78W/cm^2, (b)102W/cm^2, (c)120W/cm^2, (d)139W/cm^2, (e)160W/cm^2, (f) 206W/cm^2

When the heat flux increased, more confined hydrophobic islands were activated and thus number of nucleation sites increased (see Figure 6). Resistance of ITO heater was used to represent the surface temperature in Fig. 6 because ITO has linear relationship between resistance and temperature for previous studies.

According to Figures 5 & 6, it can be concluded that the effect of heat transfer enhancement was resulted from several particular bubble behaviors on a hydrophilic-hydrophobic patterned surface. They were summarized as: confined nucleation sites, bubble growth, bubble interaction and unique shapes of bubble.

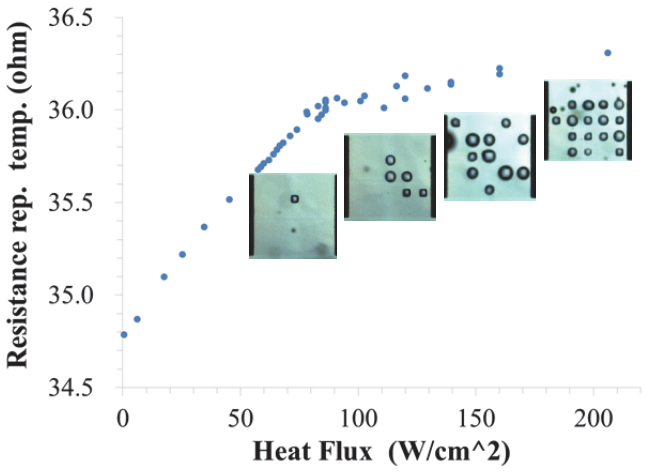

Figure 6 Nucleation sites vs. heat flux

Bubble Dynamics and Breakup

Figure 7(a) shows the nucleation boiling and bubble dynamics, when a bubble nucleates on a hydrophilic (left) or hydrophobic (right) surface. The contact angle (θ), as seen in Figure 7(a), is the angle at which the liquid-vapor interface meets the solid-liquid interface. The contact angle is determined by the resultant between adhesive and cohesive forces, which control the tendency of a bubble to growth and depart over a flat. Many studies of the wettability effects on heat transfer were focused on a pool boiling heat transfer area, including heterogeneous nucleation, nucleate boiling heat transfer and critical heat flux (CHF). Wang & Dhir [24] reported the results that the good surface wettability causes a decrease of the density of active nucleation sites. Most of two-phase heat transfer mechanisms are highly related with a contact angle hysteresis due to the dynamics motion of the interface. The contact angle hysteresis is affected by a degree of heterogeneity and roughness of the solid surface [25]. Phan et al. [12, 26] investigated the wettability effects on a nucleate boiling using various materials deposited on surfaces. In the hydrophobic surface, no bubble departure was noticed and the heat transfer was unstable when the bubbles stayed on the heating surface. In the hydrophilic surface, they measured a departure diameter and a bubble emission frequency. They concluded that increasing the contact angle, the bubble departure diameter is decreased and the decreased contact angle is resulted in the increases of both a bubble growth time and a waiting period of the next bubble. Therefore, the highest heat transfer coefficient would be obtained with a surface of which the contact angle of is either 0º or 90º. However, in contrast, Harada et al. [27] reported that the bubbles were lifted-off the vertical heated surface of a small contact angle within a shorter period of time after the nucleation than that of a larger contact angle.

Another important issue in a pool boiling heat transfer system is the wettability effects on the critical heat flux (CHF). Near the CHF situation, if the surface has ability to supply liquid to evaporate, the CHF can be increased. However, because in pool boling situation, only natural convection flow can help the liquid supply in a very limited effect, then vapor bubble can cover the entire surface which resulted in decreasing the CHF. Gaertner [28] reported that a low contact angle results in the higher value of CHF, while a high contact angle results in the lower value of CHF. In the other words, the highly wetting surface, which is a lower contact angle, enhances the CHF of the pool boiling. Recently, based on the CHF enhancement of the micro/nano structured superhydrophilic surface, many researchers have been trying to obtain the CHF enhanced surface [29-32].

However, in the previous studies, the static contact angles surround the triple contact lines were assumed to be uniform, i.e. the surface has a uniform wettability. Betz *et al.* [13] proposed a wettability patterned surface for enhancing heat transfer in pool boiling. Because the critical wavelength λ for initiating this instability of bubble columns on a plain surface can be calculated by Taylor instability:

$$\lambda = 2\pi\sqrt{\frac{3\sigma}{g(\rho_l - \rho_v)}} \qquad (1)$$

According to Zuber (1959), the dry-out responsible for CHF is caused by Helmoltz instability that merges individual bubble columns. The critical vapor velocity that triggers Helmoltz instability is inversely proportional to $\lambda^{-0.5}$, therefore, the critical heat flux for water on plain surface can be estimated as

$$\dot{q}_c'' \propto \left(\frac{1}{\lambda}\right)^{0.5} \approx 110 W/cm^2 \qquad (2)$$

On a wettability patterned surface, the wettability patterns of the pitch network will induce instability of near wall flow (see later part this paper) and, therefore, it will constraint the wavelength of instability to the pitch of network, p. Under this hypothesis, therefore, the factor *f* for CHF enhancement can be calculated according to the geometry parameters given by Betz et al. [13]:

$$f \propto \left(\frac{\lambda}{p}\right)^{0.5} \Rightarrow 11 \text{ to } 23 \qquad (3)$$

Furthermore, as shown in Figure 7(b), on a wettability patterned smooth surface, the contact angle becomes asymmetric around different contact lines. The unequal interfacial surface tension at different contact lines will force the micro vapor bubble to move from the hydrophilic surface to the hydrophobic surface, which will generate local convective microflow along the surface. This will further enhance the heat transfer coefficient in pool boiling.

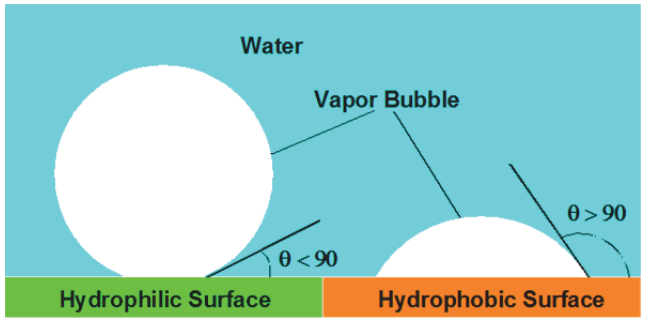

(a)

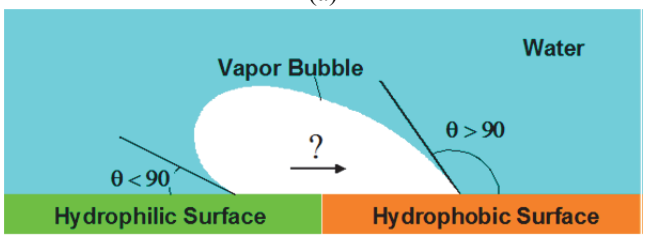

(b)

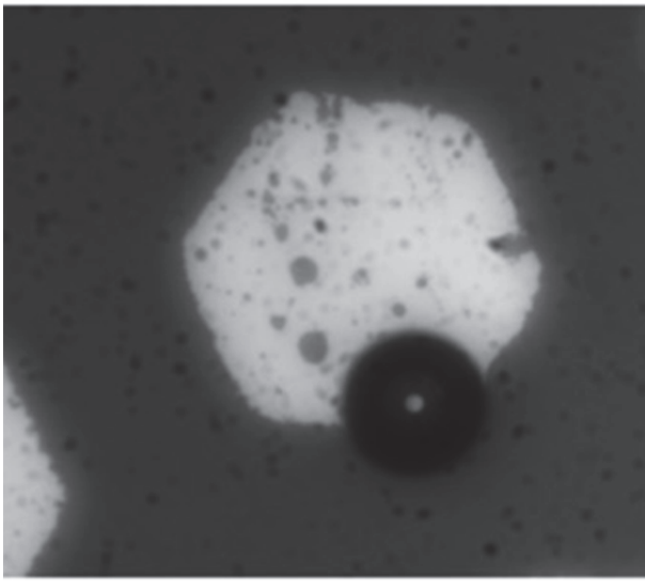

(c)

Figure 7 Nucleation Boiling and Bubble Dynamics, (a) bubble nucleation on a hydrophobic or a hydrophilic surface; (b) proposed model of bubble nucleation at the interface between areas of different wettability; (c) Experimental result by Betz et al (2010)

Because, in most cases, nucleation will happen at the at the interface between areas of different wettability, as demonstrated by Betz *et al* [13], the flow boiling and pool boiling in the local microsurfaces become with some similarities.

Bubble Coalescence

When more than one bubble merged into one, the shape of the merged bubble was quite different from that on uniform surfaces. For a hydrophilic or hydrophobic surface, bubbles are almost spherical while for patterned surface, the shapes are unique resulting from the heterogeneous of surface wettability. The contact line under the bubble was more likely to shift from hydrophilic network to the edge of the hydrophobic islands which is also the reason why identical bubbles on patterned surface are always confined on islands.

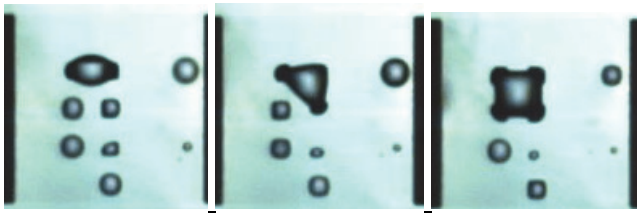

Figure 8 Bubble coalescence with increasing numbers of identical bubbles with heat flux of 139W/cm^2

When there were more than one bubble on the surface, the neighboring bubbles will interact with each other (see Figure 8). Two, three, four and more identical bubbles merging into one bigger bubble was observed in the experiments as shown in Figure 9. It was noted that, bubbles merged and broke from time to time in this study while bubbles would merged, grew bigger and departed finally from smooth surfaces. The reason was that the surrounding hydrophilic regions constrained the contact diameter of the merged bubble and induced instability to the bubble.

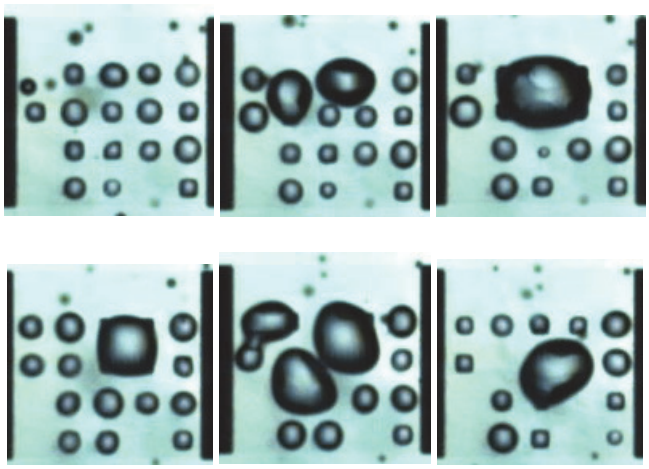

Figure 9 Bubble coalescence on a patterned surface with heat flux of 206W/cm^2

It was also found that some micro droplets were formed under the nucleation bubble during the pool boiling process, which will further prevent the dry-out from high heat flux.

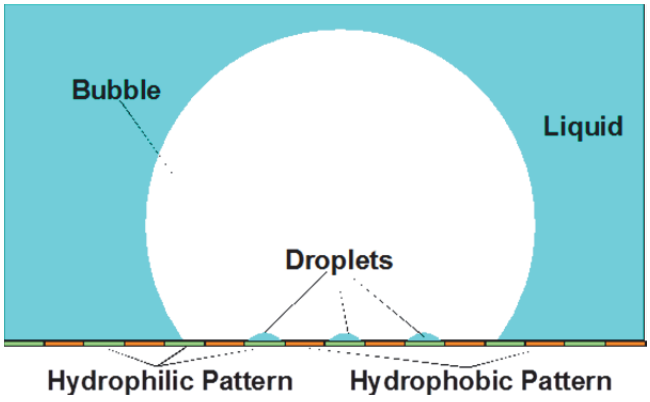

Figure 10 Droplets under a vapor bubble in pool boiling

Results on microstructured surfaces:

The test results are shown in Figure 11 for comparison. For micro wettability patterned surfaces, both Betz et al and our ITO patterned glass show a significant enhancement over the plain surface. In our case, the heat flux can reach as high as 300W/cm^2 with simple wettability patterns.

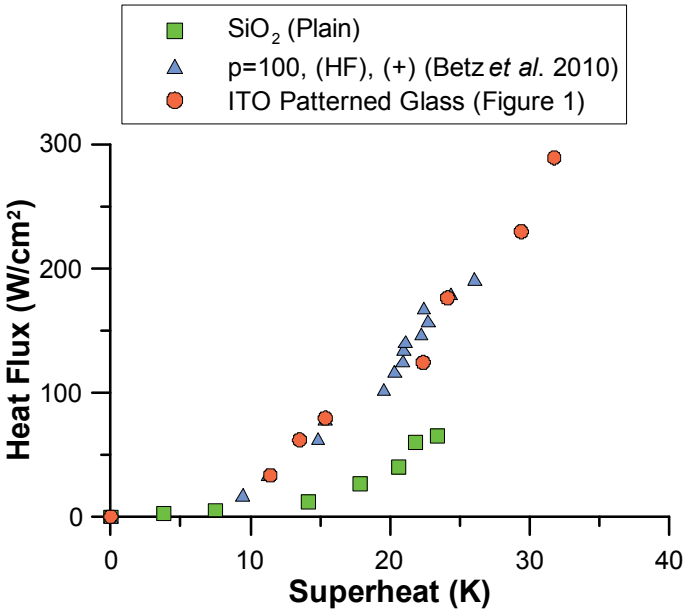

Figure 11 Surface temperatures via heat fluxes with different surface properties

FLOW BOILING ON MICRO/NANOSTRUCTED SURFACES IN A MICROCHANNEL

Wettability patterned surface induced vortex flows

To study the fluid flow on a wettability patterned surface in a microchannel, we studied a 3-D wettability patterned surface in a capillary tube first. A very thin photoresist layer (PR204) inside the round tubes was deposited by controlling the drying rate of the photoresist utilizing the recently developed techniques [33]. By using microfabrication technologies, a patterned photoresist film is successfully developed inside the round capillary tubes, as described in Figure 12. After formation of patterned PR, Octadecyltrichlorosilane (OTS) is employed to form a self-assembled monolayer (SAM) [34, 35] on the surfaces without the protection of photoresist patches. Acetone is then used to get rid of the photoresist film and OTS patches covered on the tube walls are kept unchanged. Patterns are therefore obtained, and the surfaces have heterogeneous surface charge density when they contact with electrolytes. Zeta potential, a parameter to describe surface charge property, of the tube surfaces with uniform OTS coating is measured to be -120mV with the current monitoring method [36].

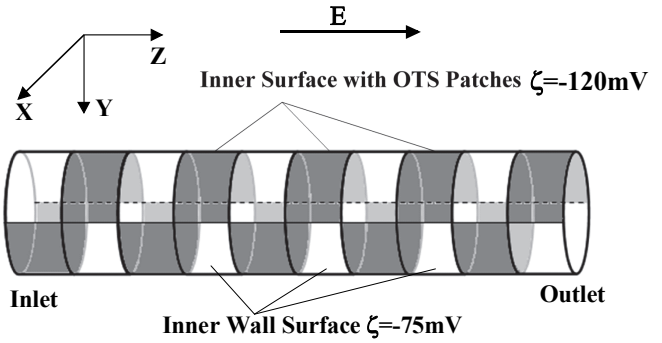

Figure 12 Schematic of a 3D wettability patterned surface in a round capillary tube

Based on the samples fabricated shown in Figure 12, numerical analysis were conducted using CFD code (CFD-ACE+ Inc.). In the simulation, the fluid is assumed Newtonian and incompressible. Because the electric double layer is extremely thin, its relaxation and distortion are not considered [33]. The electrophoretic mobility of species is assumed to be zero. The flow field with an external electric field of 5 V/mm driving the liquid near the wall flowing from the left side to the right and having an internal pressure difference pushing the liquid at the center of the tube flowing in a reverse direction is investigated. Figure 13 shows the calculated flow field under above mentioned conditions.

It is obvious that some vortices start from the beginning of the OTS patches and end at the border between the OTS and the wall. According to Figure 13, the rolling fluid of vortex flow is in the region of the blocks A and B which is near the borders of patches. The flow fields, therefore, were measured experimentally utilizing a micro resolution particle image velocimetry (μPIV) as shown in Figure 13. Both numerical simulation and experimental validation show the wettability induced vortex flow near the interface between areas of different wettability. This wettability induced flow may affect both pool boiling and flow boiling conditions. Although in this

study, an external electric potential was applied the driving the flow, it will be confirmed in the later session that even without electric potential applied, the vortex flow will also induced by wettability patterned surfaces.

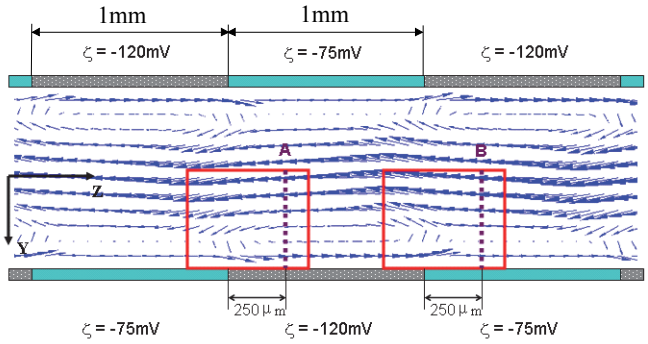

Figure 13 Wettability patterns induced vortex flows

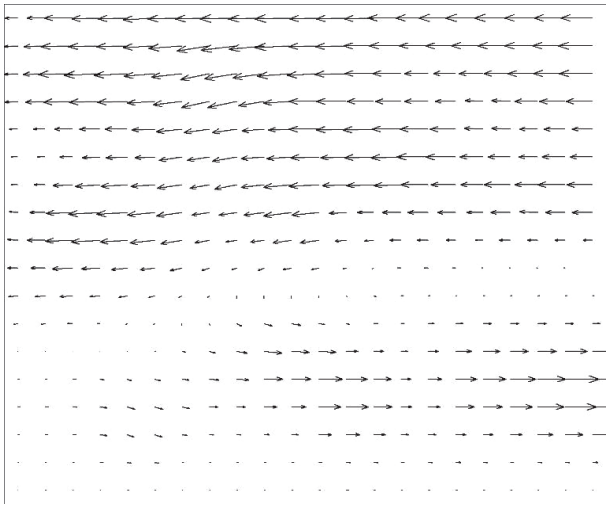

Figure 14 Micro PIV measurements of wettability patterns induced vortex flows near position **A** in Figure 12.

Fabrication of wettability patterned microchannles

To study bubble dynamics and heat transfer on wettability patterned surfaces in a microchannel, as shown in Figure 15, a microchannel device consisting of a single microchannel, two manifolds for inlet and outlet port, and a series of temperature sensors and heater on the back side of chip was fabricated.

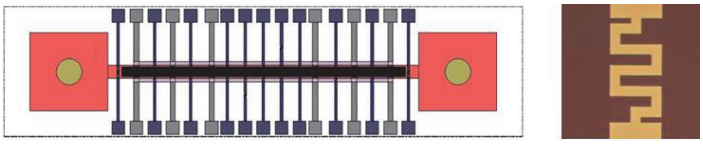

(a) (b)

Figure 15 Wettability patterned microchannel (a) Layout of chip design and (b) temperature sensor

The typical shape of microchannel has a hydraulic diameter 88.2 μm and the length of microchannel is 10mm. A simple overview of this device fabrication is given as follows. Firstly a photolithography technology was used to get the pattern of microchannel and manifolds on a silicon wafer, then the wafer was immersed the Tetramethylammonium hydroxide (TMAH) solution(25%, 80°C) to generate the microchannel and inlet and outlet manifolds with the depth 50 μm. A surface profiler was employed to measure the dimension of microchannel. Secondly the inlet and outlet ports on the backside were etched using the deep reactive ion etching (DRIE) process. Finally four steps of lift-off process were adopted to form sensor array and microheater. The first step is to coat 3 μm thickness photoresist uniformly using the spray coating technology. A stand photolithography process was used to form the sensor pattern. After that, 50nm thickness Ti/W and 200nm platinum (Pt) metal layer were sputtered on the patterned surface in sequence. Using the ultrasonic pool and acetone and IPA to strip the photoresist, sensor array can be generated on the wafer backside, another standard lift-off process was used to fabricate the gold connect pad with thickness of 200nm. Simultaneously another standard two steps of lift-off process were used to form the microheater part. It should be noted that, before fabrication of the microheater part, a layer of 1μm silicon oxide was deposited on the top of sensor array which is used to insulate the circuit between sensor array and microheater.

To get the precise temperature distribution along the microchannel bottom surface, the Pt sensors should be calibrated prior to boiling experiments. Calibration process was performed in a mechanical convection oven with précised temperature control as shown in Figure 16. Good linearity indicates an accurate temperature measurement results can be obtained using these sensors.

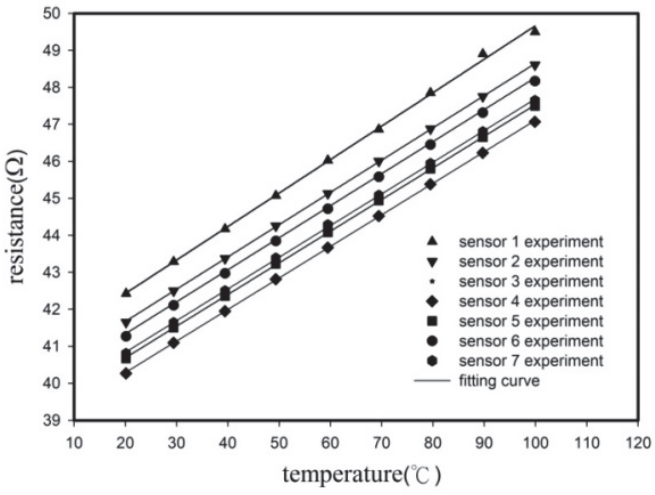

Figure 16 The calibration curves between platinum resistance and temperature

In the present experiment, the hydrophilic parts are silicon dioxide, and the hydrophobic surfaces were fabricated utilizing

Teflon AF400 on the oxide surface. Using photolithography technology, the hydrophobic microdots were patterned on the oxide surface as shown in Figure 17. During the fabrication process, a simple method was employed to examine the different wettability of hydrophilic and hydrophobic parts. A little hot air was blowing onto the wafer surface, as shown in Figure 17, and then tiny droplets will appear on the microchannel surface because of condensation. It is easy to identify that condensed droplets are disparate with smaller droplets on the hydrophobic parts than hydrophilic parts. It is difficult to measure the contact angle (CA) of the microchannel surface. However the CA of bulk surface of silicon dioxide and Teflon coated surface was measured to have 33° and 120°, respectively.

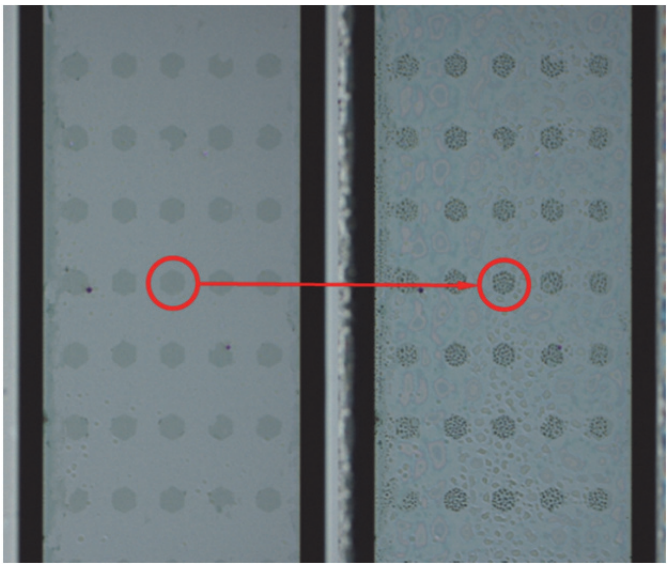

Figure 17 Droplet condensations on patterned surfaces

Experimental setup

The microchannel chip was packaged with a pre-designed holder with Swagelok tube fittings. A Harvard pump was used to syringe degassed deionized water into the microchannel chip with a precise and constant mass flux. The Pt sensors resistance and voltage loaded on heater were collected by a data acquisition system (Agilent: module 34972). The visualization system includes a high speed camera (Redlake HG-100K) and a Nikon microscope (Eclipse 80*i*). A DC power supply was employed to provide voltage on the heater. Firstly the deionized water was degassed by vigorous boiling for two hours. Flow boiling conditions was setup by an increasing heat flux and constant flow rate. In the experiments, the flow rate was 5ml/h and the velocity of water in microchannel was 0.059m/s. The voltage was changed gradually with an interval of 1V, however if onset of boiling was happened in the microchannel, this interval will be smaller in order to occurrence of critical heat flux. The procedures were described as followings. First flow rate was set on the syringe pump at a desired rate. After several minutes the flow in the microchannel can achieve a steady state. Secondly turn on the DC power supply and wait ten minutes, and then collect the data including Pt sensor and voltage. Thirdly change the voltage and redo the second step.

Bubble dynamics and fluid flow in microchannels

As the input heating power was increased gradually, the nucleation boiling in the fluid flow can occur in the microchannel. As shown in Figure 18, a sequence of high speed images had given the different results between bare silicon and patterned surfaces in microchannels. The most distinguished character is the microdroplets condensation on microchannels during boiling processes. It is evidence to see that condensation droplet size on patterned surface is smaller than bare silicon surface. It means that when bubble generation due to heat flux on the microchannel surface, there are more nucleation condensation sites on patterned surfaces, it indicates that the temperature drop on patterned surface should be larger than bare silicon. Also it is worth noting that, on the patterned surface, it is easier to generate vapor because of continuously heating processes. These aforementioned characters should elucidate the later heat transfer performance with a better result on the patterned surface reasonably.

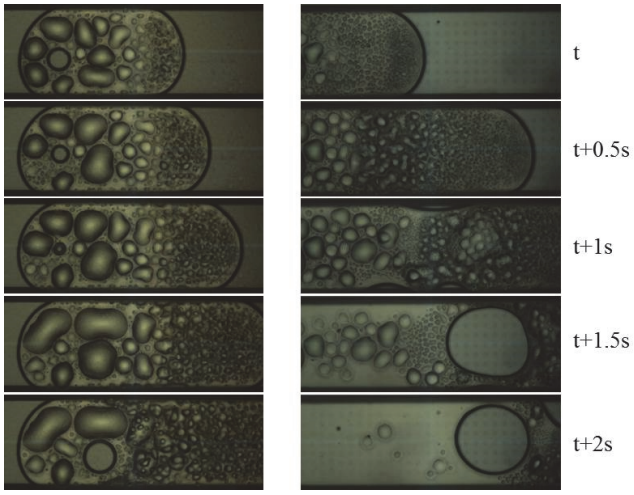

Figure 18 Flow pattern comparisons between bare silicon (left side) and patterned surface (right side)

Simultaneously μPIV was employed to measure the velocity distribution with case of bubble growing process as shown in Figure 19. It seems that the liquid phase bypass the small bubble smoothly at the stage of bubble growing early stage. However it is interesting to point out that a rotational velocity was found along the bubble edge as demonstrated in the Figure 19 (b).

Heat Transfer Enhancement in Flow Boiling

The measured heat transfer and temperature results are shown in Figures 20 and 21, respectively. From Figure 20(a), it is easy to see that heat flux does not have distinguish disparity between bare silicon and patterned surface, it could indicate that heterogeneous surface (wettability) has no effect on single phase heat transfer in such case. However at two phase flow

regime (flow boiling), where, the microchannel backside wall temperature (located as T4) was selected as representative to character the whole chip, it seems that the patterned surface has a better heat transfer performance, which also can be reflected in Figure 20(b) with higher HTC on the patterned surface microchannel. The temperature is illustrated in Figure 21(a) and (b) for the flow condition with flow rate 5ml/h and the inlet fluid temperature is fixed at about 30 ^{o}C. It is evident to see that the temperature is higher in the bare silicon microchannel, which means that the HTC is lower than the patterned surface microchannel. In current experiments, the periodic temperature fluctuation is not fierce as reported in many papers due to the lower heat flux on chip and the heat removal capacity for a single channel.

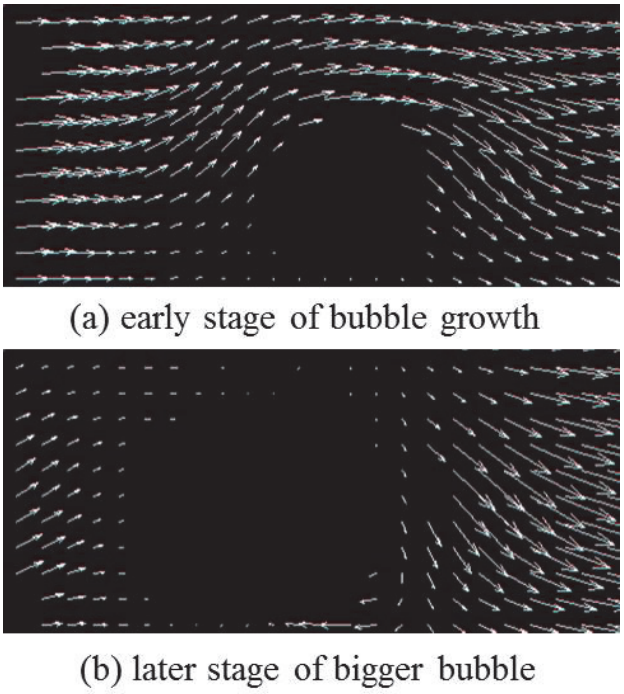

Figure 19 μPIV measurements of flow passing a growing bubble

MICRO/NANOSTRUCTURED HEAT SPREADER WITH ASYMMETRICAL WETTABILITY PATTERNS

Fabrication Techniques

In this section, we present a novel heat spreader with wettability surface modification. In comparison with a conventional one, the major difference is by replacing the conventional wick-laid upper wall with a super-hydrophobic condensing wall and the evaporator with nanostructured copper sphere surfaces. Figure 22 illustrates the working principle of our novel vapor chamber.

Heat is inputted through the wall and wick structure from the center bottom, the working fluid absorbs heat and is vaporized. When reaching the cold upper wall, the vapor condenses quickly forming a droplet and dropping down directly from the super-hydrophobic wall. This super-hydrophobic surface has several advantages: (1) It can effectively prevent the generation of a liquid film that may significantly degrade the condensation efficiency; (2) the vapor can easily condense to a droplet on this surface, which then drops down directly into the wick. This can shorten the water feeding route and prevent dry-out in the center wick. The nanostructure and wettability of the condenser surface is shown in Figure 23 and 24 respectively.

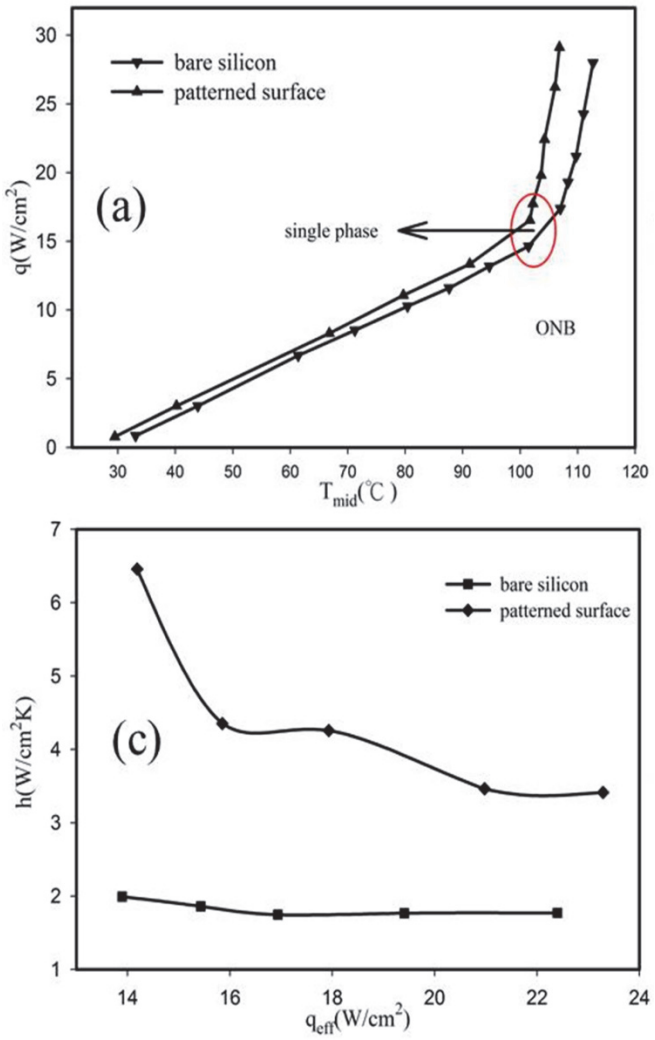

Figure 20 Heat transfer comparison between bare silicon and wettability patterned surface microchannels (a) boiling curve based with the middle sensor, (b) heat transfer coefficient in the two phase boiling regime

A LW-9510 vapor chamber thermal performance measurement apparatus was used to test the performance of the vapor chamber. The experimental setup is shown in Figure 25. Heat was inputted from the heater by an external power supply. An aluminum block with an area of 170×80mm^2 was placed on the top of the vapor chamber when the experiment was carried out. Recirculated cooling water went through the aluminum block to dissipate the heat and the cooling temperature was set

to be 35°C. Five T-type thermocouples were allocated on the outside top surface of vapor chamber and another one inserted into the heater block to measure the heater temperature which is shown in Figure 25.

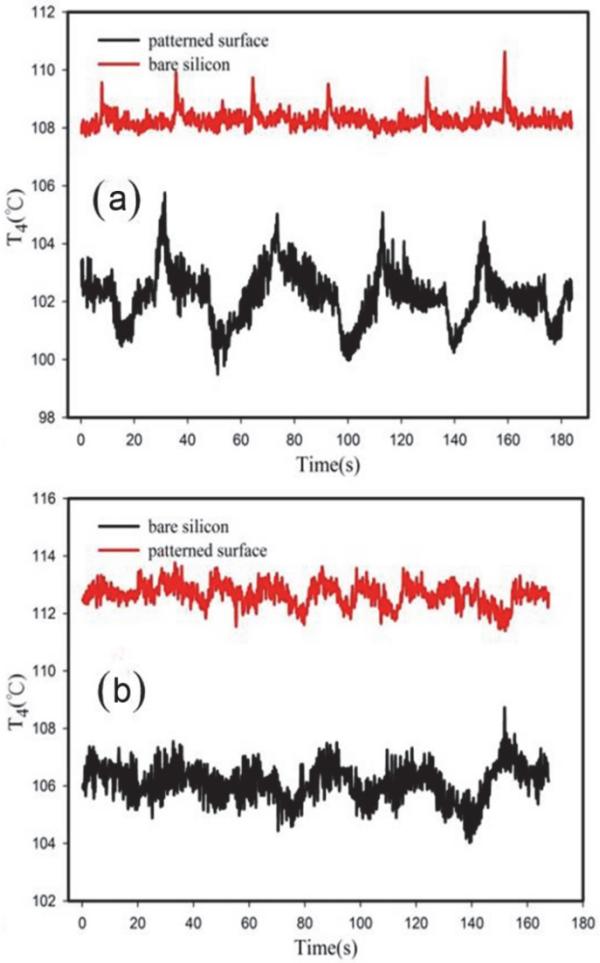

Figure 21 (a) Temperature fluctuation under the condition of heat flux 17.37W/cm^2 for bare silicon and 17.73 W/cm^2 for patterned surface, (b) Temperature fluctuation under the condition of heat flux 27.99 W/cm^2 for bare silicon and 26.22 W/cm^2 for patterned surface. The flow rate is fixed at 5ml/h.

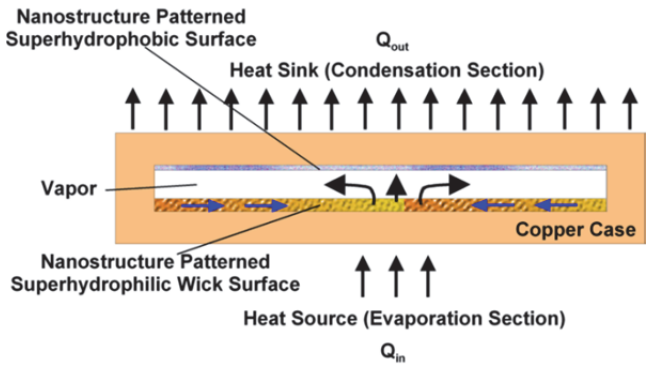

Figure 22 Asymmetric vapor chamber with super-hydrophobic condensing and super-hydrophilic evaporating walls

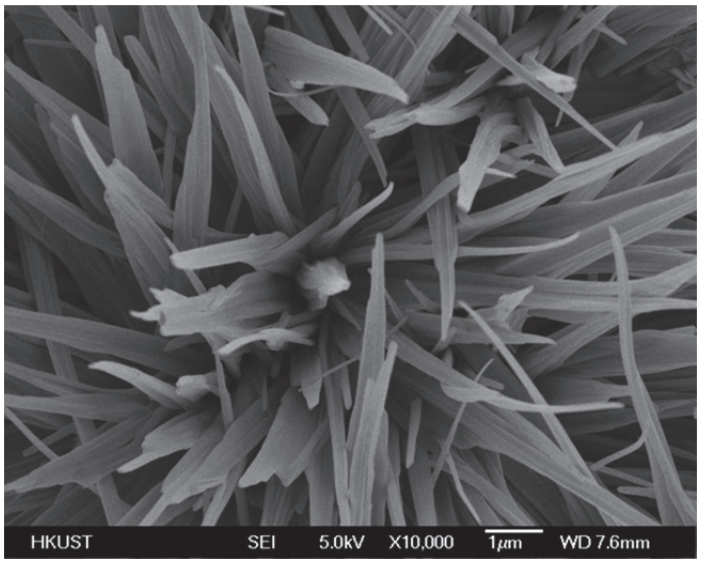

Figure 23 The nanostructured condenser surface before coating with FAS

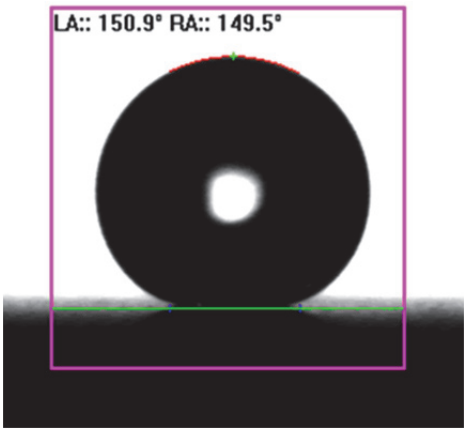

Figure 24 Wettability of nanostructured condenser surface after coating with FAS

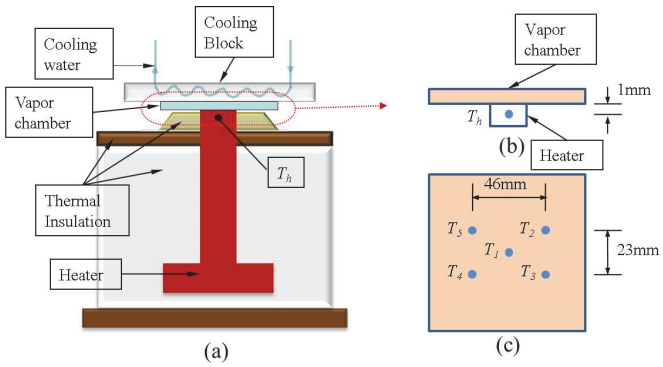

Figure 25 Experimental Setup: (a) experimental apparatus; (b) heater temperature measurement; (c) thermocouple distribution on the outside surface of the vapor chamber

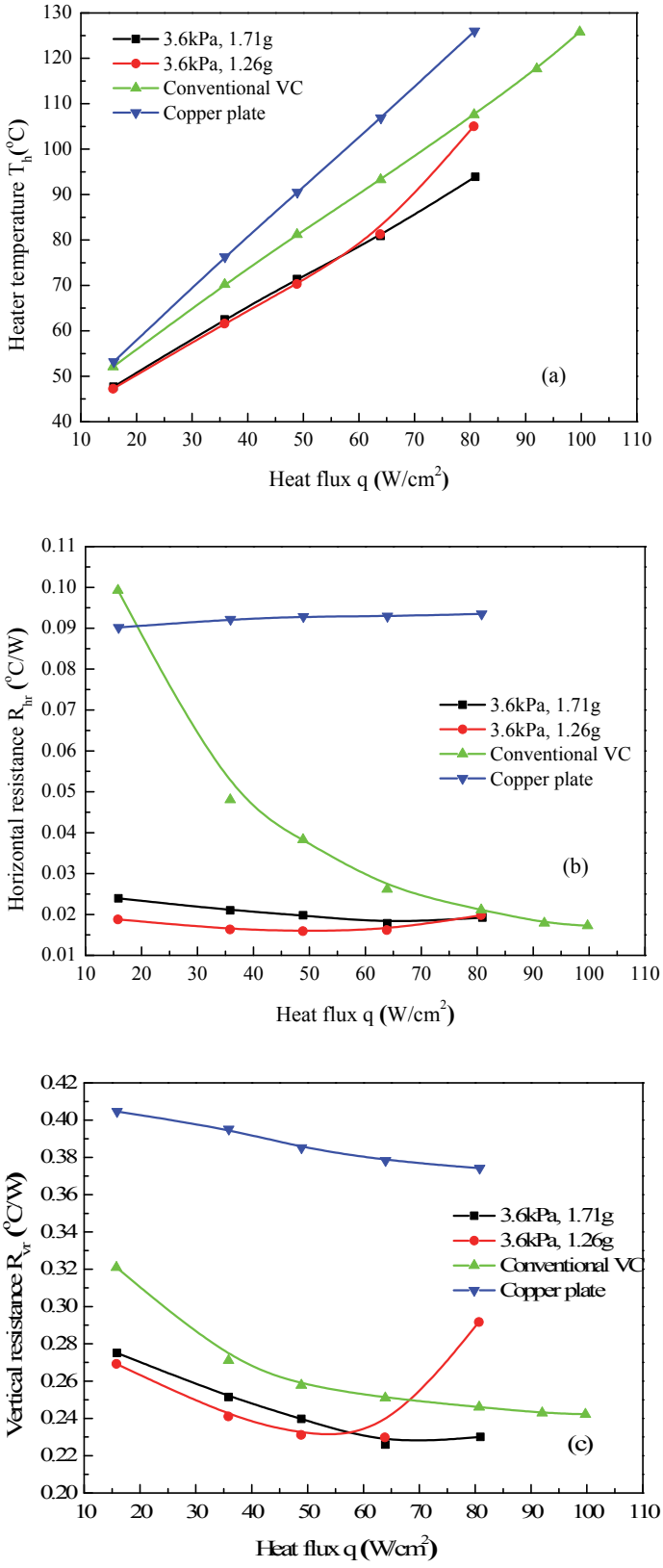

Figure 26 Performance of the nanostructured asymmetric vapor chamber compared with the conventional vapor chamber and copper plate

Results and Discussion

Figure 26(a) shows the heater temperature T_h varies against the heat flux q. For the novel vapor chamber, T_h is slightly lower when the amount of charging water is less. However, this situation reverses after the heat flux exceeds 65W/cm^2. But the novel vapor chamber with either amount of charging water shows a much lower T_h, compared with the conventional vapor chamber and copper plate, especially when the heat flux is relatively large. This can be explained as follows: for the conventional vapor chamber, the homogenous wick is sintered on the inner wall; when the vapor reaches the condenser wick, it condenses and spreads to form a thin film in the wick. This layer of thin film will prevent the further condensation. This kind of condensation is known as film condensation. However, the condenser wick is replaced by the super-hydrophobic nanostructured surface in the novel vapor chamber. When the vapor reaches this kind of super-hydrophobic surface, it condenses into droplets, due to the low surface energy on this kind of surface. When the droplets grow bigger, they will either fall down to the evaporator or be absorbed by the sintered wick structure in the evaporator. The water drainage is much more efficient than that of the conventional vapor chamber; and the heat transfer coefficient of this kind of drop-wise condensation is much larger than that of film condensation. As a result, more heat is removed and the heater temperature is lower at the same heat flux in the novel vapor chamber. Because the phase change heat transfer is much more efficient than conduction, both the conventional and novel vapor chambers show a better performance than the copper plate to reduce the heater temperature. From this figure, we find that the temperature differences between the novel vapor chamber and conventional vapor chamber and copper plate can reach 15℃ and 30℃ respectively. This indicates that the novel vapor chamber can greatly reduce heater temperature.

Figure 26(b) shows the relationship between horizontal resistance R_{hr} and heat flux q. For the novel vapor chamber, R_{hr} is slightly smaller when the charging water is less. Rhr decreases slightly with the increase of q, compared with the conventional vapor chamber. However, the tendency of horizontal resistance for copper plate is opposite with the increase of heat flux. For both charging amounts of water, R_{hr} of the novel vapor chamber is smaller than that of the conventional vapor chamber; especially it is much smaller than that of the copper plate. As a result, a more uniform temperature distribution can be achieved for the novel vapor chamber.

Figure 26(c) shows the vertical resistance R_{vr} as a function of heat flux q. R_{vr} decreases with the increase of q for the three kinds of heat spreader. For the novel vapor chamber, R_{vr} is slightly lower when the amount of charging water is less. However, a transition occurs when the heat flux exceeds 60W/cm^2. This can be explained as the critical heat flux for our less charging vapor chamber is reached at this value. As a result, a huge temperature jump appears and causes an increment on R_{vr}. In general, R_{vr} of the novel vapor chamber is smaller than that of the conventional vapor chamber; especially it is much smaller than that of the copper plate. For q is 65W/cm^2, the

novel vapor chamber can reduce the vertical resistance by about 65%, compared with the copper plate.

Figure 27 shows the relationship between the heat flux and the temperature difference across the evaporator and condenser layers (ΔT) of the newly designed vapor chamber. It indicates that this newly designed vapor chamber can sustain a heat flux that is slightly above 220W/cm^2. However, heat fluxes greater than 220W/cm^2 was not tested since the resulting heater temperature would exceed the safe value which is set to be 160^{o}C. However, we can predict from the trend of the curve that the critical heat flux (CHF) of this active cooling spreader has the potential to be larger than 220W/cm^2. This enhancement on the CHF must be attributed to the multi-layers of the wick structure in the evaporator and the nano-structure patterned super-hydrophobic condenser surface.

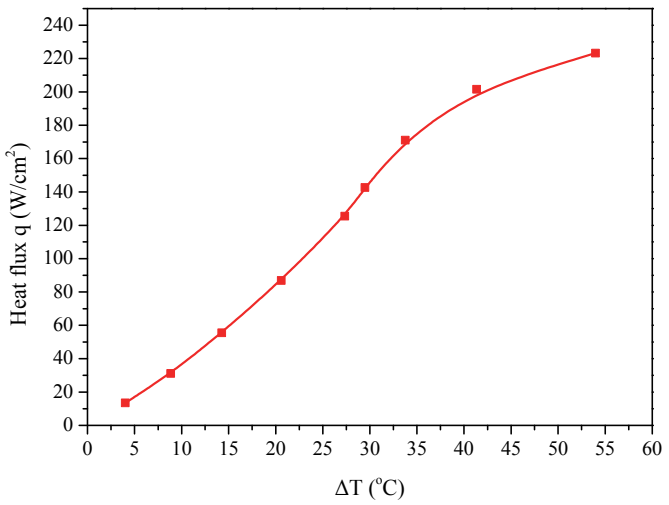

Figure 27 Thermal performance of the newly designed vapor chamber (Initial vapor chamber pressure = 3.6kPa)

CONCLUSION

In this paper, the challenges and opportunities of wettability patterned micro/nanostructure surfaces on boiling heat transfer and fluid flow have been discussed. Bubble dynamics, fluid flow and heat transfer caused by the wettability patterned micro/nanostructure surfaces have been reported and discussed. The effects of micro/nanostructure patterned surfaces on flow generation under a vapor bubble in a microchannel under very low Reynolds number have been demonstrated.

Following synergetic effects can enhance heat transfer coefficient (HTC) and at the same time increase the critical heat flux (CHF) for pool boiling and flow boiling:

- The wettability patterns of the pitch network will induce instability of near wall flow and, therefore; it will constraint the wavelength of instability to the pitch of network, p, which will increase the critical heat flux.
- On a wettability patterned microstructure surface, the number of bubble nucleation sites is significantly larger than a plain surface. Bubble coalescence and break-up can be controlled by this kind confined nucleation.
- On wettability patterned smooth surfaces, the capillary force act on the line of contact (also called triple line) become asymmetric around the bubble. The unequal interfacial surface tension at different lines of contact will force the micro vapor bubble to move from the hydrophilic surface to the hydrophobic surface, which will generate local convective microflow along the surface.
- The wettability patterns can induce vortex flow near the interface between areas of different wettability. This wettability induced flow may affect both pool boiling and flow boiling conditions.
- In pool boiling and flow boiling on a wettability patterned micro/nanostructure surface, droplet condensation inside of a growing vapor bubble can be observed. These droplets will help to prevent the dry-out at high critical heat flux.
- The vapor condensation inside a bubble with patterned surface is more effective than bare silicon which enhances the heat transfer.
- A micro/nanostructured heat spreader with asymmetrical wall wettability will be demonstrated. This improvement not only results in drop-wise condensation which has a much higher heat transfer coefficient compared with film condensation, but also provides a shortcut for the condensed water to drop back directly to the center wick

ACKNOWLEDGEMENT

This research is supported by the Research Grants Council (RGC) of the Government of the Hong Kong Special Administrative Region (HKSAR) with Project Nos. 618210 and 617812.

REFERENCES

[1] S. G. Kandlikar, Scale effects on flow boiling heat transfer in microchannels: A fundamental perspective, Int. J. of Thermal Science, Vol.49, pp. 1073-1085, 2010

[2] S. G. Kandlikar, Nucleation characteristics and stability considerations during flow boiling in microchannels, Exp. Thermal and Fluid Science, 30, pp. Vol. 441-447, 2006

[3] S. G. Kandlikar, Fundamental issues related to flow boiling in minichannels and microchannels, Exp. Thermal and Fluid Science Vol. 26, pp.389-407, 2002

[4] C. J. Kuo, Y. Peles, Local measurement of flow boiling in structured surface microchannels, Int. Journal of Heat and Mass transfer, Vol.50, pp.4513-4526, 2007

[5] Kosar, Y. Peles, Boiling heat transfer in a hydrofoil-based micro pin fin heat sink, Int. Journal of Heat and Mass transfer, Vol. 50, pp.1018-1034, 2007

[6] S. Krishnamurthy, Y. Peles, Flow boiling of water in a circular staggered micro-pin fin heat sink, Int. Journal of Heat and Mass transfer, Vol. 51, pp.1349-1364, 2008

[7] J. Y. Lee, M. H. Kim, M. Kaviany, S. Y. Son, Bubble nucleation in microchannel flow boiling using single

artificial cavity, Int. Journal of Heat and Mass transfer, Vol. 54, pp.5139-5148, 2011

[8] K. M. M. Morshed, F. Yang, M. Y. Ali, J. A. Khan, C. Li, Enhanced flow boiling in a microchannel with integration of nanowires, Applied Thermal Engineering, Vol.32, pp.68-75, 2012

[9] D. Li et al, Enhanced flow boiling heat transfer in microchannels for thermal management with monolithically-integrated silicon nanowires, Nano Letters, Vol.12, pp.3385-3390, 2012

[10] T. Y. Liu, P. L. Li, C.W. Liu, C. Gau, Boiling flow characteristics in microchannels with very hydrophobic surface to superhydrophilic surface, Int. Journal of Heat and Mass transfer, Vol. 54, pp. 126-134, 2011

[11] C. Choi, J. S. Shin, D. I. Yu, M. H. Kim, Flow boiling behaviors in hydrophilic and hydrophobic microchannels, Experimental Thermal and Fluid Science Vol. 35, pp.816-824, 2011

[12] Phan, H. T, Cabeny, N., Marty, P., Colasson, S., & Gavillet, J., Surface wettability control by nanocoating: The effects on pool boiling heat transfer and nucleation mechanism. *Int. J. Heat Mass Transfer*, Vol. 52, pp. 5459-5471, 2009.

[13] Betz, A. R., Xu, J., Qiu, H. H., Attinger, D., Do surfaces with mixed hydrophilic and hydrophobic areas enhance pool boiling? *Applied Physics Letters*, 97, pp.141909-1-3, 2010.

[14] Carey V., Liquid-Vapor Phase Change Phenomena, Taylor & Francis, London, 1992

[15] Nam, Y. and Ju, Y. S. Appl. Phys. Lett. 93, 103115, 2008.

[16] Weibel, J. A., Garimella, S. V., and North, M. T., Int. J. Heat Mass Transfer 53, 4204, 2010.

[17] Chien, L. H. and Webb, R. L., Exp. Therm. Fluid Sci. 16, 332 , 1998.

[18] Li, C., Wang, Z., Wang, P. I., Peles, Y., Koratkar, N., and Peterson, G. P., Small 4, 1084,2008.

[19] Chen, R. Lu, M.-C., Srinivasan, V., Wang, Z., Cho, H. H., and Majumdar, A. Nano Lett. 9, 548, 2009.

[20] S. Kim, H. D. Kim, H. Kim, H. S. Ahn, H. Jo, J. Kim, and M. H. Kim, Exp. Therm. Fluid Sci. 34, 487, 2010.

[21] Dhir V. K. and Liaw, S. P., J. Heat Transfer 111, 739,1989.

[22] Wang, C. H. and Dhir, V. K., J. Heat Transfer 115, 670 , 1993.

[23] B. J. Jones, J. P. McHale, and S. V. Garimella, J. Heat Transfer 131, 121009, 2009.

[24] Wang, C. H. and Dhir,V. K. J. Heat Transfer 115, 659 ,1993.

[25] Johnson Jr., R. E. and Dettre, R. H., Wettability and contact angle. Surface and Colloid Science, Vol. 2, pp. 85-153, 1969.

[26] Phan, H. T., Caney, N., Marty, P., Colasson, S., & Gavillet, J., How does surface wettability influence nucleate boiling? C.R. Mecanique, Vol. 337, pp. 251-259, 2009.

[27] Harada, T., Nagakura, H., & Okawa, T., Dependence of bubble behavior in subcooled boiling on surface wettability. Nuclear Engineering and Design, Vol. 240, pp. 3949-3955, 2010.

[28] Gaertner, R. F., Photographic Study of Nucleate Pool Boiling on Horizontal Surface. ASME J. Heat Transfer, Vol. 87, pp. 17-29, 1965.

[29] Kim, S. Kim, H. D., Kim, H., Ahn, H. S., Jo, H., Kim, W., & Kim, M. H., Effects of nano-fluid and surfaces with nano structure on the increase of CHF, Exp. Therm. Fl. Sci., Vol. 4, pp. 487-495, 2010.

[30] Ahn, H. S., Lee, C., Kim, H., Jo, H., Kang, S., Kim, W., Shin, J., & Kim, M. H., Pool boiling CHF enhancement by micro/nanoscale modification of Zircaloy-4 surface. Nuclear Engineering and Design, Vol. 240, pp. 3350-3360, 2010.

[31] Truong, B., Hu, L., Buongiorno, J., & Mckrell, T., Modification of sandblasted plate heaters using nanofluids to enhance pool boiling critical heat flux. Int. J. Heat Mass Transfer, Vol. 53, pp. 85-94, 2010.

[32] Forrest, E., Williamson, E., Buongiorno, J., Hu, L., Rubner, M. & Cohen, R., Augmentation of nucleate boiling heat transfer and critical heat flux using nanoparticle thin-film coatings. Int. J. Heat Mass Transfer, Vol. 53, pp. 58-67, 2010.

[33] Zhang P. and Qiu H.-H. (2008): Investigation of Patterned Surface Modification on 3D Vortex Flows Generation in a Micropipe, J. of Micromechanics and Microengineering, 18 (2008) 115030.

[34] Tripp C P and Hair M L 1992 An infrared study of the reaction of octadecyltrichlorosilane wit silica, *Langmuir* 8, 1120-1126

[35] Breen T L, Tien J, Oliver S R J, Hadzic T and Whitesides G M 1999 Design and self-assembly of open, regular, 3D mesostructures, *Science* 284, 948-951

[36] Sze A, Erickson D, Ren L and Li D Q 2003 Zeta-potential measurement using the smoluchowski equation and the slope of the current-time relationship in electroosmotic flow, *J. Colloid Interface Sci.* 261, 402-410